Contrib. Astron. Obs. Skalnaté Pleso **52/2**, 58 – 71, (2022)
https://doi.org/10.31577/caosp.2022.52.2.58

The interaction between hyperons and the surface gravitational redshift of proto neutron star PSR J0740+6620

Xian-Feng Zhao

School of Sciences, Southwest Petroleum University, Chengdu, 610500, China
(E-mail: zhaopioneer.student@sina.com)

Received: August 1, 2022; Accepted: October 8, 2022

Abstract. An effect of the contributions from σ^* and ϕ mesons on the surface gravitational redshift of PNS PSR J0740+6620 is studied with relativistic mean field theory in consideration of a baryon octet. We find that the energy density ε increases relative to the same pressure p as the contributions from σ^* and ϕ mesons are taken into account. Relative to the same central energy density, the radius R of the PNS increases while the mass M, the mass radius ratio M/R and the surface gravitational redshift z of the PNS decrease, taking into account the contributions from σ^* and ϕ mesons. Under the constraint of mass M=2.08 $\mathrm{M}_\odot$, considering the contributions from σ^* and ϕ mesons, for the PNS PSR J0740+6620, the radius decreases by about -0.08%, the central energy density increases by about 0.89%, the central pressure increased by about 0.76%, the mass radius ratio increases by about 0.08%, and the surface gravitational redshift increases by about 0.17% from z=0.31663 to z=0.31718.
Key words: stars: binaries - general: stars

1. Introduction

Neutron stars (NSs) are extremely dense because of their large mass M and small radius R (Glendenning, 1997). The mass of an NS will provide constraints on its properties. For example, the mass of an NS would constrain the symmetry energy within it (Li et al., 2021), and perhaps the properties of an NS could also be explained by dark matter (Ding et al., 2022).

Whenever a new massive NS is found, it will inevitably provide some new restrictions on the properties of NS matter. In recent years, several massive NSs have been discovered in succession. In 2010, NS PSR J1614-2230 was observed (Demorest et al., 2010; Fonseca et al., 2016) and three years later another more massive NS PSR J0348+0432 was found (Antoniadis et al., 2013). In 2019, NS PSR J0740+6620 was observed, possibly the most massive NS to date, with a mass of $M = 2.14^{+0.10}_{-0.09}$ $\mathrm{M}_\odot$ (2020) (Cromartie et al., 2020), or $M = 2.08^{+0.07}_{-0.07}$ $\mathrm{M}_\odot$ (2021) (Fonseca et al., 2021). Why NS PSR J0740+6620 has such a large mass can be explained by scalar tensor theories of gravity by Degollado et al (Degollado et al., 2020). The mass of NS PSR J0740+6620 suggests that the equation of state (EoS) of NS matter must be hard enough, and it rules out some EoSs that are too soft (Zhou et al., 2019). Since NS PSR J0740+6620 is much more massive than an NS of mass 1.4 $M_\odot$, it is much denser than an NS of mass 1.4 $M_\odot$ (Han et al., 2020).

The mass radius ratio M/R of an NS determines its surface gravitational redshift z. If we know the mass radius ratio M/R of an NS we can calculate its surface gravitational redshift z, and vice versa. NSs are relatively easy to observe. So if we know the surface gravitational redshift z of an NS and the mass of the NS, we can calculate its radius R. It can be seen that the surface gravitational redshift z of an NS is an important physical quantity to describe the properties of an NS (Glendenning, 1997).

An NS is formed from a proto neutron star (PNS) that emit energy through neutrino radiation. The PNS is formed in the center of a supernova explosion due to gravitational collapse. A PNS can have temperatures as high as T=30 MeV. The theoretical study of PNSs is helpful to understand the evolution of NSs (Burrows et al., 1986; Prakash et al., 1997).

The interaction between nucleons in PNS matter can be described in terms of σ, ω and ρ mesons. However, the interaction between the hyperons, which can be described in terms of mesons $f_0(975)$ (denoted as σ^*) and $\phi(1020)$ (denoted as ϕ), must also have some effect on the properties of the PNS matter (Schaffner et al., 1994; Mu et al., 2017).

In this paper, we study the effect of the contributions from σ^* and ϕ mesons on the surface gravitational redshift of the PNS PSR J0740+6620 using the relativistic mean field (RMF) theory (Zhou, 2016).

2. RMF theory of finite temperature NS matter

The Lagrangian density of finite temperature NS matter (Glendenning, 1997; Schaffner et al., 1994) is

$$\begin{aligned}\mathcal{L} = & \sum_B \overline{\Psi}_B(i\gamma_\mu\partial^\mu - m_B + g_{\sigma B}\sigma + g_{\sigma^* B}\sigma^* \\ & -g_{\omega B}\gamma^0\omega - g_{\phi B}\gamma^0\phi - g_{\rho B}\gamma^0\tau_3\rho)\Psi_B \\ & -\frac{1}{2}m_\sigma^2\sigma^2 - \frac{1}{3}g_2\sigma^3 - \frac{1}{4}g_3\sigma^4 \\ & +\frac{1}{2}m_\omega^2\omega^2 + \frac{1}{2}m_\rho^2\rho^2 - \frac{1}{2}m_{\sigma^*}^2\sigma^{*2} + \frac{1}{2}m_\phi^2\phi^2 \\ & + \sum_{\lambda=e,\mu} \overline{\Psi}_\lambda\left(i\gamma_\mu\partial^\mu - m_\lambda\right)\Psi_\lambda. \end{aligned} \tag{1}$$

The energy density and the pressure of mesons and baryons (Glendenning, 1987a,b) are respectively

$$\begin{aligned}\varepsilon &= \frac{1}{2}m_\sigma^2\sigma^2 + \frac{1}{2}m_{\sigma^*}^2\sigma^{*2} + \frac{1}{3}g_2\sigma^3 + \frac{1}{4}g_3\sigma^4 \\ &+\frac{1}{2}m_\omega^2\omega_0^2 + \frac{1}{2}m_\phi^2\phi^2 + \frac{1}{2}m_\rho^2\rho_{03}^2 \\ &+\sum_B \frac{2J_B+1}{2\pi^2}\int_0^\infty \kappa^2 n_B(k)\mathrm{d}\kappa\sqrt{\kappa^2+m_B^{*2}},\end{aligned} \tag{2}$$

$$\begin{aligned}p &= -\frac{1}{2}m_\sigma^2\sigma^2 - \frac{1}{2}m_{\sigma^*}^2\sigma^{*2} - \frac{1}{3}g_2\sigma^3 - \frac{1}{4}g_3\sigma^4 \\ &+\frac{1}{2}m_\omega^2\omega_0^2 + \frac{1}{2}m_\phi^2\phi^2 + \frac{1}{2}m_\rho^2\rho_{03}^2 \\ &+\frac{1}{3}\sum_B \frac{2J_B+1}{2\pi^2}\int_0^\infty \frac{\kappa^4}{\sqrt{\kappa^2+m_B^{*2}}}n_B(k)d\kappa,\end{aligned} \tag{3}$$

where $n_B(k)$ is the Fermi-Dirac distribution function of baryon

$$n_B(k) = \frac{1}{1+exp\left[\left(\varepsilon_B(k)-\mu_B\right)/T\right]}. \tag{4}$$

The energy density and the pressure of leptons are respectively

$$\begin{aligned}\varepsilon &= \sum_l \frac{1}{\pi^2}\int_0^\infty \kappa^2 n_l(k)\mathrm{d}\kappa\sqrt{\kappa^2+m_l^2} \\ &+ \sum_\nu \left(\frac{7\pi^2T^4}{120} + \frac{T^2\mu_\nu^2}{4} + \frac{\mu_\nu^4}{8\pi^2}\right),\end{aligned} \tag{5}$$

$$\begin{aligned}p &= \frac{1}{3}\sum_l \frac{1}{\pi^2}\int_0^\infty \frac{\kappa^4}{\sqrt{\kappa^2+m_l^2}}n_l(k)d\kappa \\ &+ \sum_\nu \frac{1}{360}\left(7\pi^2T^4 + 30T^2\mu_\nu^2 + \frac{15\mu_\nu^4}{\pi^2}\right).\end{aligned} \tag{6}$$

The mass and radius of the PNS are obtained by the TOV equation (Tolman, 1939; Oppenheimer et al., 1939)

$$\frac{\mathrm{d}p}{\mathrm{d}r} = -\frac{(p+\varepsilon)\left(M+4\pi r^3 p\right)}{r\left(r-2M\right)}, \tag{7}$$

$$M = 4\pi\int_0^R \varepsilon r^2\mathrm{d}r. \tag{8}$$

The PNS's surface gravitational redshift can be obtained by (Glendenning, 1997):

$$z = \frac{1}{\sqrt{1-2(M/R)}} - 1. \tag{9}$$

3. Parameters

In this work, we select eight sets of nucleon coupling parameters to calculate PNSs: DD-ME1 (Typel et al., 1999), GL85 (Glendenning, 1985), GL97 (Glendenning, 1997), TW99 (Typel et al., 1999), GM1 (Glendenning et al., 1991), FSUGold (Todd-Rutel et al., 2005), FSU2R (Laura et al., 2017) and FSU2H (Laura et al., 2017). In the early stage of formation, the temperature of the PNS can be as high as 30 MeV. We choose the PNS PSR J0740+6620's temperature as T=20 MeV (Burrows et al., 1986).

Denoting hyperons Λ, Σ and Ξ) by h, we define $x_{\sigma h} = \frac{g_{\sigma h}}{g_\sigma} = x_\sigma$, $x_{\omega h} = \frac{g_{\omega h}}{g_\omega} = x_\omega$, $x_{\rho h} = \frac{g_{\rho h}}{g_\rho}$, which are in the range from 1/3 to 1 (Glendenning et al., 1991). The parameter $x_{\rho h}$ is selected by quark SU(6) symmetry (Schaffner et al., 1996; Schaffner-Bielich et al., 2000). The calculation results show that the bigger $x_{\sigma h}$ and $x_{\omega h}$ are, the bigger PNS mass is (Zhao, 2019). Therefore, in order to obtain the largest possible mass of the PNS, we must choose the largest possible hyperon coupling parameters $x_{\sigma h}$ and $x_{\omega h}$. We select $x_{\omega h}$=0.9 and $x_{\sigma h}$ can be obtained by the following formula (Glendenning, 1997)

$$U_h^{(N)} = m_n \left(\frac{m_n^*}{m_n} - 1\right) x_{\sigma h} + \left(\frac{g_\omega}{m_\omega}\right)^2 \rho_0 x_{\omega h}, \tag{10}$$

where we choose hyperon-potentials as follows $U_\Lambda^{(N)} = -30$ MeV (Weissenborn et al, 2012; Gal et al., 2016), $U_\Sigma^{(N)}$=30 MeV (Schaffner-Bielich et al., 2000; Weissenborn et al, 2012; Gal et al., 2016; Batty et al., 1997) and $U_\Xi^{(N)} = -14$ MeV (Harada et al., 2010). We choose $x_{\sigma^* h}$ and $x_{\phi h}$ as follows (Schaffner et al., 1994)

$$x_{\sigma^*\Lambda} = x_{\sigma^*\Sigma} = 0.69, x_{\sigma^*\Xi} = 1.25, \tag{11}$$

$$x_{\phi\Lambda} = x_{\phi\Sigma} = -\frac{\sqrt{2}}{3}, x_{\phi\Xi} = -\frac{2\sqrt{2}}{3}. \tag{12}$$

Without considering the contributions from σ^* and ϕ mesons, we calculate the PNS by using the above eight groups of nucleon coupling parameters, and find that only the maximum masses (denoted as M_{max}) of the PNS obtained by DD-MEI, TW99 and GM1 are greater than that of the PNS PSR J0740+6620 (see Fig. 1). Among these three sets of parameters, the mass and radius of the PNS PSR J0740+6620 given by GM1 are in agreement with the results of Fonseca et al. ($M = 2.08^{+0.07}_{-0.07}$ $M_\odot$ (Fonseca et al., 2021)) and Miller et al.(R=$13.7^{+2.6}_{-1.5}$ km (Miller et al., 2021)). Therefore, we use GM1 to study the influence of the contributions from σ^* and ϕ mesons on the surface gravitational redshift of the PNS PSR J0740+6620.

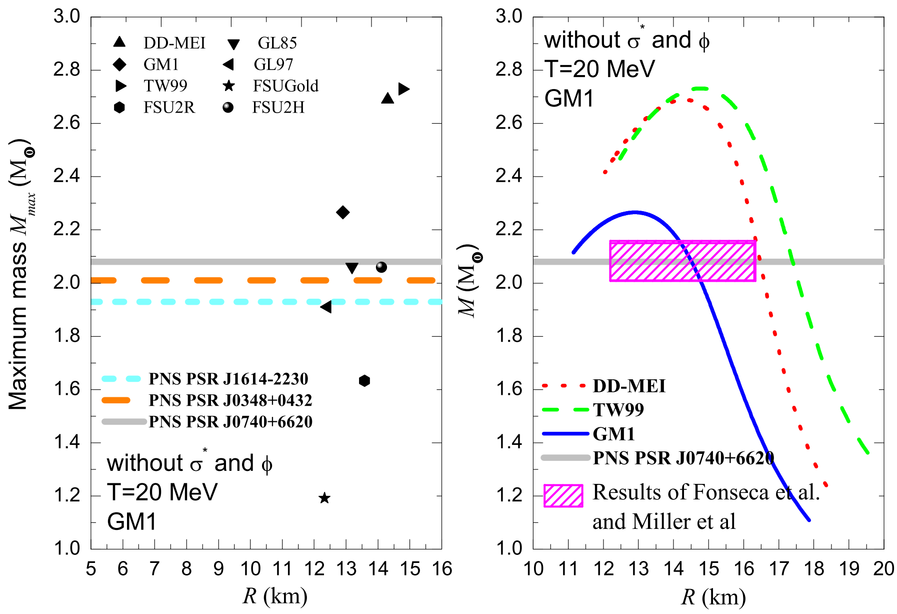

Figure 1. The relationship between the mass M or the maximum mass M_{max} of the PSR J0740+6620 and the radius R of the PNS. The contributions from σ^* and ϕ mesons are not considered in the calculation. The PNS's temperature is chosen as T=20 MeV.

4. The energy density and the pressure in the PNS PSR J0740+6620

The upper half of Fig. 2(a) shows the energy density ε of the PNS as a function of the pressure p. The lower half of Fig. 2(b) represents an enlarged view of the curve in the box in (a). The PNS's temperature is assumed to be 20 MeV. The red real curve does not consider the contributions from σ^* and ϕ mesons, while the green virtual curve does. The curve ends at the central energy density ε_c and the central pressure p_c of the PNS PSR J0740+6620.

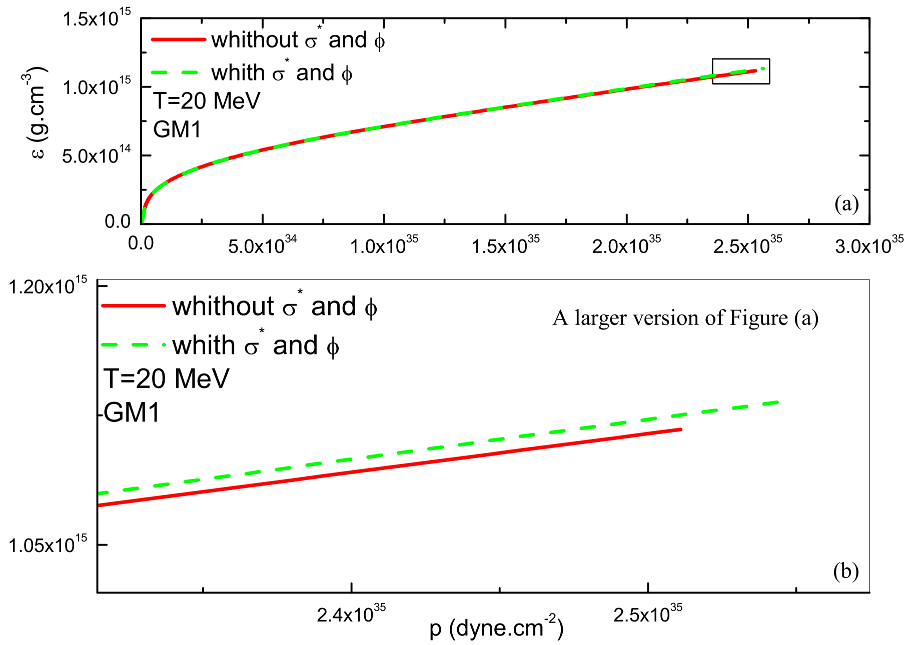

Figure 2. (a) The energy density ε of the PNS as a function of the pressure p. (b) A magnified view of the curve in the box in figure (a). The PNS's temperature is assumed to be 20 MeV. The red real curve does not consider the contributions from σ^* and ϕ mesons, while the green virtual curve does. The curve ends at the central energy density ε_c and the central pressure p_c of the PNS PSR J0740+6620.

We can see from Fig. 2(a) that the energy density ε of the PNS increases as the pressure p increases. We also see that the energy density ε increases relative to the same pressure p, taking into account the contributions from σ^* and ϕ mesons. Under the constraint of mass M=2.08 $M_\odot$, considering the contributions from σ^* and ϕ mesons, the central energy density of the PNS PSR J0740+6620 increases by about 0.89% from ε_c=1.013×10^{15} g.cm^{-3} to ε_c=1.022×10^{15} g.cm^{-3} (see Table 1); the central pressure of the PNS PSR J0740+6620 increased from p_c=2.118×10^{35} dyne.cm^{-2} to p_c=2.134×10^{35} dyne.cm^{-2}, increasing by about 0.76%.

5. The radius and the surface gravitational redshift of PNS PSR J0740+6620

The PNS's mass M and radius R as a function of the central energy density ε_c are shown in Fig. 3. The left ordinate represents the mass of the PNS, and

Table 1. The calculation results of PNS PSR J0740+6620 in this work. The mass of PNS PSR J0740+6620 is M = 2.08 $M_\odot$. ε_c, p_c, R, M/R and z are the central energy density, the central pressure, the radius, the mass radius ratio and the surface gravitational redshift of PNS PSR J0740+6620, respectively.

parameter	unit	without σ^* and ϕ	with σ^* and ϕ	percentage
ε_c	g.cm^{-3}	1.013×10^{15}	1.022×10^{15}	0.89%
p_c	dyne.cm^{-2}	2.118×10^{35}	2.134×10^{35}	0.76%
M/R	$M_\odot$/km	0.14327	0.14338	0.08%
R	km	14.518	14.507	-0.08%
z		0.31663	0.31718	0.17%

the right ordinate represents the radius of the PNS. The PNS's temperature is assumed to be 20 MeV. The red real curve does not consider the contributions from σ^* and ϕ mesons, while the green virtual curve does.

We see that the mass M of the PNS increases and the radius R decreases as the central energy density ε_c increases. Relative to the same central energy density, the mass of the PNS decreases and the radius increases, taking into account the contributions from σ^* and ϕ mesons. Under the constraint of mass M=2.08 $M_\odot$, considering the contributions from σ^* and ϕ mesons the radius of the PNS PSR J0740+6620 decreases by about -0.08% from R=14.518 km to R=14.507 km (see Table 1).

Figure 4 gives the mass radius ratio M/R and the surface gravitational redshift z of the PNS as a function of the central energy density ε_c. The PNS's temperature is assumed to be 20 MeV. The red real curve does not consider the contributions from σ^* and ϕ mesons, while the green virtual curve does. The curve ends at the central energy density ε_c and the central pressure p_c of the PNS PSR J0740+6620.

We see that the mass radius ratio M/R and the surface gravitational redshift z of the PNS all increase with the increase of the central energy density ε_c. Relative to the same central energy density ε_c, the mass radius ratio M/R and the surface gravitational redshift z of the PNS are reduced considering the contributions from σ^* and ϕ mesons. As it can also be seen from Fig. 4 and Table 1, under the limit of mass M=2.08 $M_\odot$, the mass radius ratio of PNS PSR J0470+6620 increases from M/R=0.14327 $M_\odot$/km to M/R=0.14338 by about 0.08%, and the surface gravitational redshift of PNS PSR J0470+6620 increases by about 0.17% from z=0.31663 to z=0.31718, taking into account the contributions from σ^* and ϕ mesons.

Fig. 5, Fig. 6 and Fig. 7 respectively show the variation of the surface gravitational redshift z of the PNS with the radius R, the mass M and the mass radius ratio M/R. Figure (b) in Figs. 5 and 6 are enlarged views of the curves in the boxes in corresponding figures (a), respectively. In Fig. 7, in order to sep-

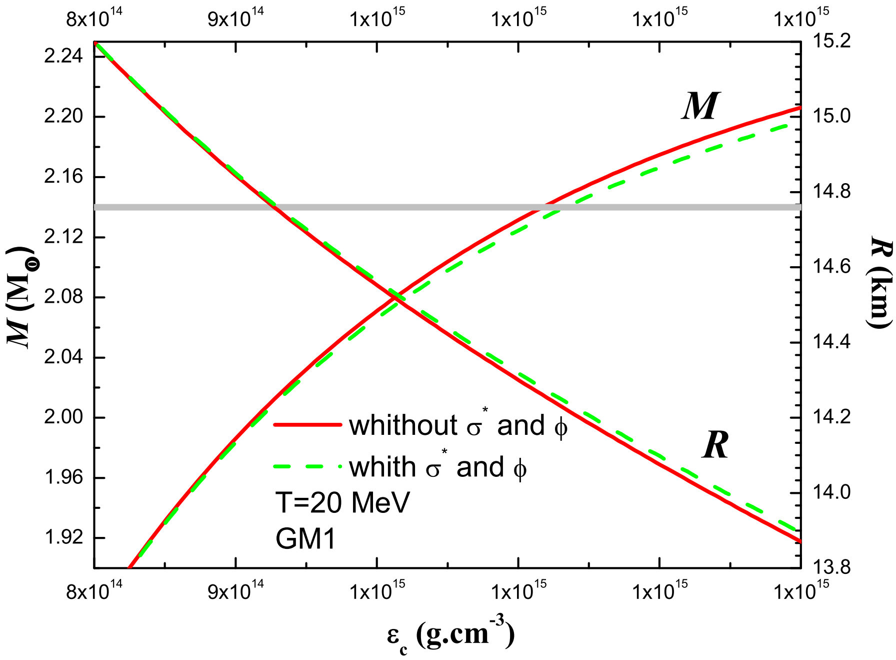

Figure 3. The PNS's mass M and radius R as a function of central energy density ε_c. The left ordinate represents the mass of the PNS, and the right ordinate represents the radius of the PNS. The PNS's temperature is assumed to be 20 MeV. The red real curve does not consider the contributions from σ^* and ϕ mesons, while the green virtual curve does.

arate the curves that take into account the contributions from σ^* and ϕ mesons and those that do not, we add 0.01 to the curve that takes into account the contributions from σ^* and ϕ mesons, that is, $z \to z + 0.01$.

Relative to the same radius R, the surface gravitational redshift z of the PNS decreases, taking into account the contributions from σ^* and ϕ mesons (see Fig. 5). Similarly, given the contributions from σ^* and ϕ mesons, the surface gravitational redshift z of the PNS increases relative to the same mass M (see Fig. 6). As it can also be seen from Fig. 7, considering the contributions from σ^* and ϕ mesons, the surface gravitational redshift of the PNS does not change with respect to the same mass radius ratio M/R, which can be known by formula (9).

In addition, under the constraint of mass M=2.08 $M_\odot$, the radius R of PNS PSR J0740+6620 will decrease, and the mass-radius ratio M/R and surface gravitational redshift z of PNS PSR J0740+6620 will increase (see Fig. 5, Fig. 6, Fig. 7 and Table 1).

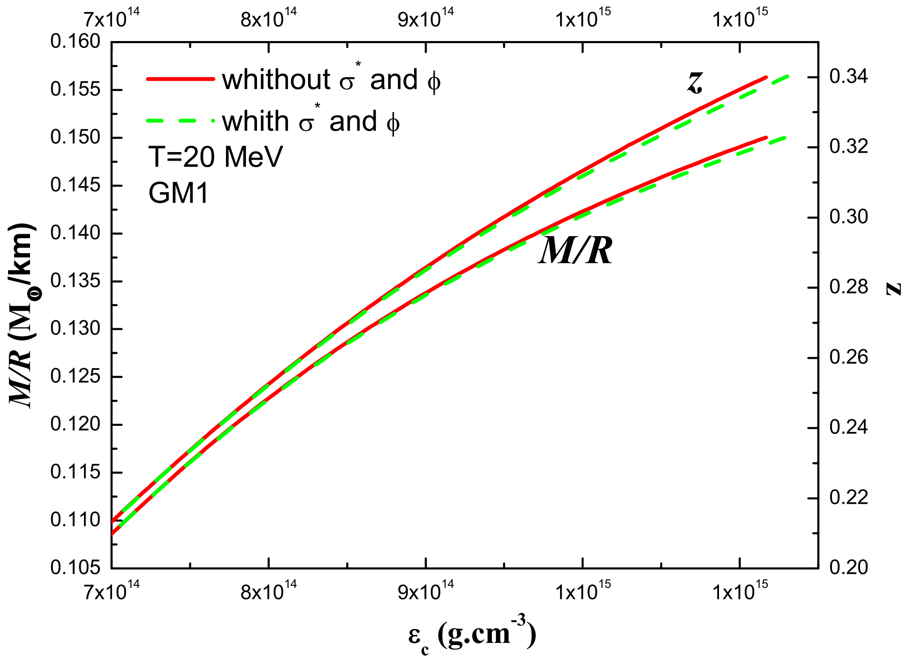

Figure 4. The mass radius ratio M/R and the surface gravitational redshift z of the PNS as a function of the central energy density ε_c. The PNS's temperature is assumed to be 20 MeV. The red real curve does not consider the contributions from σ^* and ϕ mesons, while the green virtual curve does. The curve ends at the central energy density ε_c and the central pressure p_c of the PNS PSR J0740+6620.

Given the mass of the PNS PSR J0740+6620 by Fonseca et al. (Fonseca et al., 2021), and the radius by Miller et al. (Miller et al., 2021), we can calculate the mass radius ratio to be 0.1233 $\mathrm{M}_\odot$/km$<M/R<$0.1762 $\mathrm{M}_\odot$/km and the surface gravitational redshift of the PNS PSR J0740+6620 to be $0.2541<z<0.4440$ (see the shaded boxes in Fig. 5-Fig. 7). It can be seen that our calculated results are in good agreement with the observed values.

The above results are valid for spherically symmetric static PNSs. For a rotating NS, the maximum mass increases by about 20%, and the NS becomes axisymmetric (Cook et al., 1994). The gravitational redshift of a rotating NS is a little more complicated than the previous NS as static and spherically symmetric, where we need to consider the polar redshift z_p, the equatorial redshift in the backward direction z_b, and the quatorial redshift in the forward direction z_f (Tu et al., 2022).

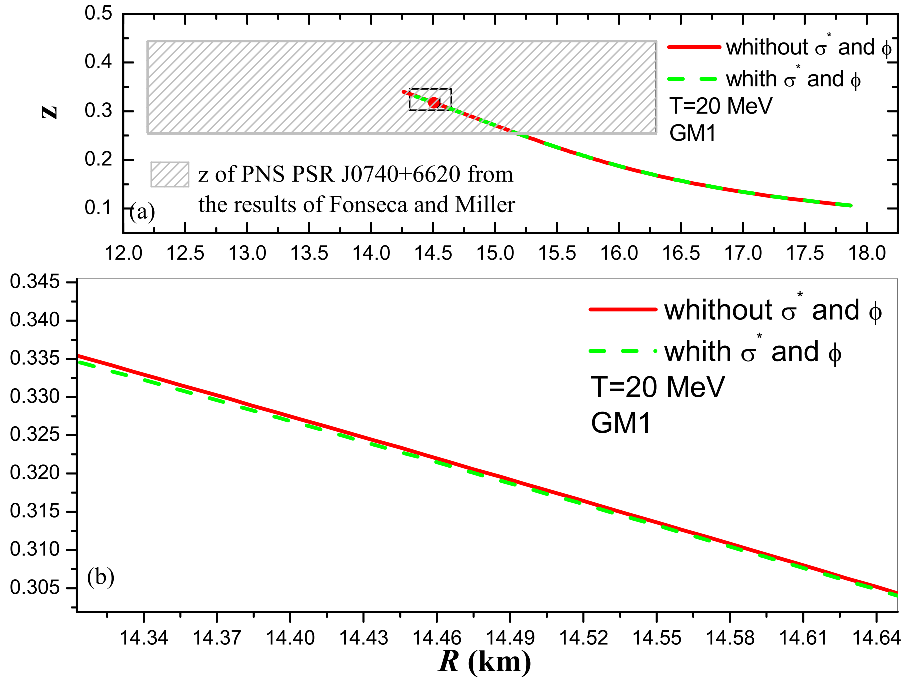

Figure 5. (a) The PNS's surface gravitational redshift z as a function of the radius R. (b) A magnified view of the curve in the box in figure (a). The PNS's temperature is assumed to be 20 MeV. The red real curve does not consider the contributions from σ^* and ϕ mesons, while the green virtual curve does. The curves end at the radius R of the PNS PSR J0740+6620.

6. Summary

We studied the effect of the contributions from σ^* and ϕ mesons on the surface gravitational redshift of PNS PSR J0740+6620 with RMF theory in consideration of a baryon octet. Here, we use eight sets of nucleon coupling constants GL85, GL97, GM1, DD-MEI, TW99, FSUGold, FSU2R and FSU2H to calculate the PNS. The temperature of the PNS is chosen as T=20 MeV. We find that only three of them (DD-MEI, GM1 and TW99) can give the PNS PSR J0740+6620's mass. We use GM1 to describe the PNS PSR J0740+6620.

The energy density ε of the PNS increases as the pressure p increases. The PNS's radius R decreases while the mass M, the mass-radius ratio M/R and the surface gravitational redshift of PNS increase with the increase of the central energy density ε_c.

The energy density ε increases relative to the same pressure p, taking into

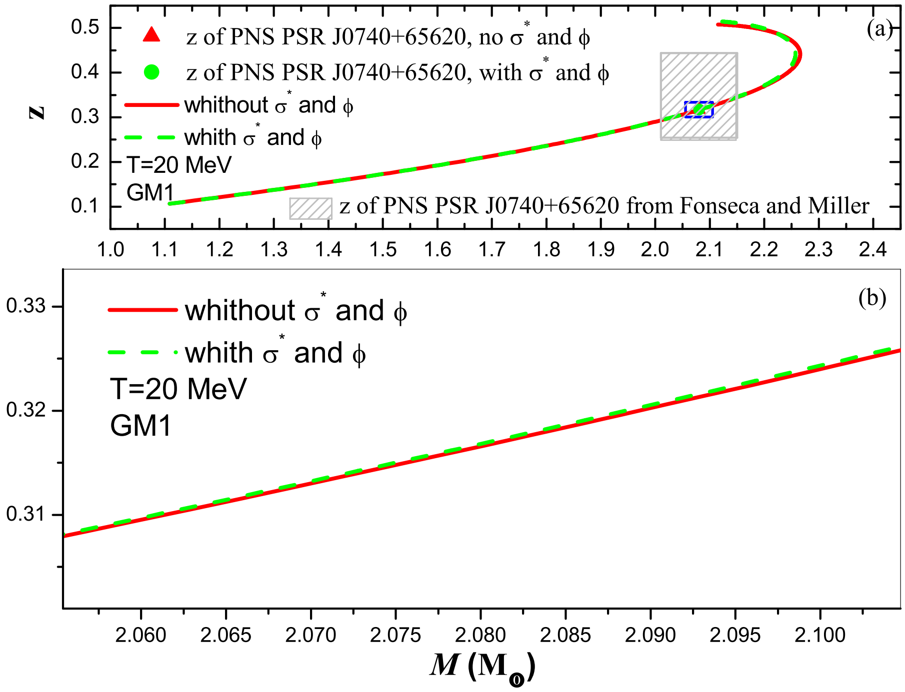

Figure 6. (a) The PNS's surface gravitational redshift z as a function of the mass M. (b) A magnified view of the curve in the box in figure (a). The PNS's temperature is assumed to be 20 MeV. The red real curve does not consider the contributions from σ^* and ϕ mesons, while the green virtual curve does.

account the contributions from σ^* and ϕ mesons. Relative to the same central energy density, the radius R of the PNS increases while the mass M, the mass-radius ratio M/R and the surface gravitational redshift z of the PNS decrease, taking into account the contributions from σ^* and ϕ mesons.

Under the constraint of mass M=2.08 $M_\odot$, considering the contributions from σ^* and ϕ mesons, for the PNS PSR J0740+6620, the radius decreases by about -0.08% from R=14.518 km to R=14.507 km, the central energy density increases by about 0.89% from ε_c=1.013×10^{15} g.cm^{-3} to ε_c=1.022×10^{15} g.cm^{-3}, the central pressure increased by about 0.76% from p_c=2.118×10^{35} dyne.cm^{-2} to p_c=2.134×10^{35} dyne.cm^{-2}, the mass radius ratio increases from M/R=0.14327 $M_\odot$/km to M/R=0.14338 by about 0.08%, and the surface gravitational redshift increases by about 0.17% from z=0.31663 to z=0.31718.

Taking into account the contributions from σ^* and ϕ mesons, the surface gravitational redshift z of the PNS decreases relative to the same radius R, and

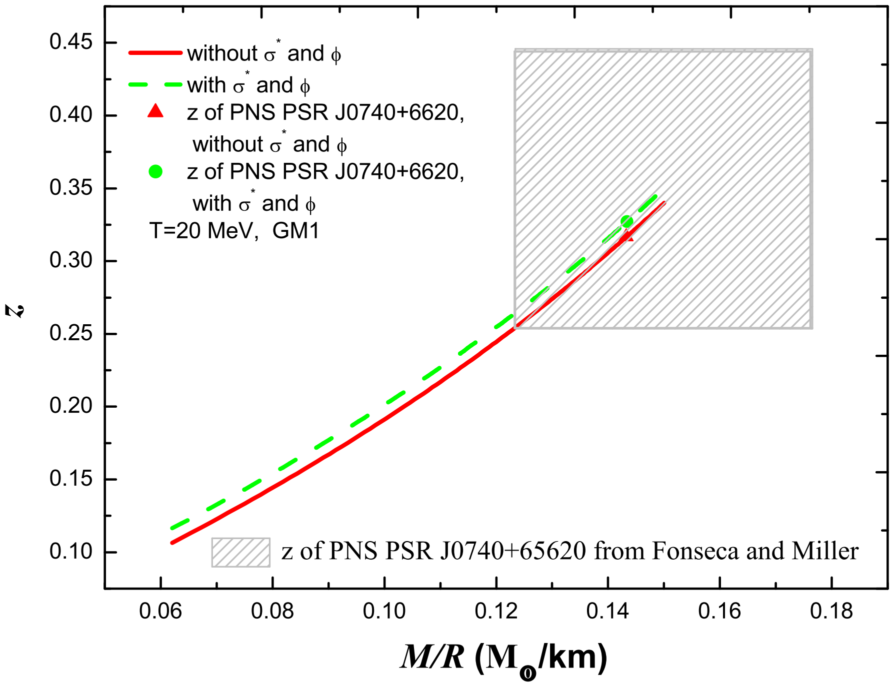

Figure 7. The PNS's surface gravitational redshift z as a function of the mass radius ratio M/R. The PNS's temperature is assumed to be 20 MeV. The red real curve does not consider the contributions from σ^* and ϕ mesons, while the green virtual curve does. The curves end at the mass radius ratio M/R of the PNS PSR J0740+6620. In order to separate the curves that take into account the contributions from σ^* and ϕ mesons and those that do not, we add 0.01 to the curve that takes into account the contributions from σ^* and ϕ mesons, that is, $z \rightarrow z + 0.01$.

increases relative to the same mass M, but does not change with respect to the same mass-radius ratio M/R

After accounting for the contributions of σ^* and ϕ mesons, the radius and surface gravitational redshifts are slightly changed compared to the case without σ^* and ϕ mesons. But the changes are too small to be inferred from astronomical observations.

Acknowledgements. This work was supported by the Natural Science Foundation of China (Grant No. 11447003).

References

Antoniadis J., Freire P.C.C., Wex N., et al. 2013, *Science*, 340, 448

Batty C.J., Friedman E., Gal A. 1997, *Phys. Rev.*, 287, 385

Burrows,A., Lattier,J.M. 1986, *Astrophys.*, **307**, 178

Cook,G.B., Shapiro,S.L., Teukolsky,S.A., 1994, *Astrophys.J.*, **424**, 823

Cromartie,H.T., Fonseca,E., Ransom,S.M., et al. 2020, *Nat.Astron.*, **4**, 72

Degollado, J.C., Salgado, M., Alcubierre, M.: 2020, *Phys. Lett.*, **B808**, 135666

Demorest,P.B., Pennucci,T., Ransom,S.M., et al. 2010, *Nature*, **467**, 1081

Ding, W.B., Cai, M.D., Chan A.H., Xu, Y.: 2022, *Int.J.Mod.Phys.*, **A37**, 2250034

Fonseca,E., Pennucci,T. T., Ellis,J.A., et al. 2016, *Astrophys. J.*, **832**, 167

Fonseca,E., Cromartie,H.T., Pennucci,T.T., et al. 2021, *Astrophys. J. Lett.*, **915**, L12

Gal,A., Hungerford,E.V., Millener,D.J. 2016, *Rev.Mod.Phys.*, **88**, 035004

Glendenning,N.K. 1985, *Astrophys. J.*, **293**, 470

Glendenning,N.K. 1987, *Phys.Lett.B*, **185**, 275

Glendenning,N.K. 1987, *Nucl.Phys.A*, **469**, 600

Glendenning,N.K. 1997, Compact Stars: Nuclear Physics, Particle Physics, and General Relativity (Springer-Verlag, New York, Inc)

Glendenning,N.K., Moszkowski,S.A. 1991, *Phys.Rev.Lett.*, **67**, 2414

Han, S., Prakash, M. 2020, *Astrophys.J.*, **899**, 164

Harada,T., Hirabayashi,Y., Umeya,A. 2010, *Phys.Lett.*, **B690**, 363

Laura,T., Mario,C., Angels,R. 2017, *Publ.Astron.Soc.Aust.*, **34**, e065

Li, Y.X., Chen, H.Y., Wen, D.H., Zhang, J. 2021, *Eur.Phys.J.*, **A57**, 31

Miller,M.C., Lamb,F.K., Dittmann,A.J., et al. 2021, *Astrophys. J. Lett.*, **918**, L28

Mu, X.L., Jia, H.Y., Zhou, Z., Wang, H.: 2017, *Astrophys.J.*, **846**, 140

Oppenheimer,J.R., Volkoff,G.M. 1939, *Phys.Rev.*, **55**, 374

Prakash,M., Bombaci,I., Prakash,M., et al. 1997, *Phys. Rep.*, **280**, 1

Schaffner,J., Dover,C.B., Gal,A., et al. 1994, *Ann.Phys.*, **235**, 35

Schaffner,J., Mishustin,I.N. 1996, *Phys.Rev.*, **C53**, 1416

Schaffner-Bielich,J., Gal,A. 2000, *Phys.Rev.*, **C62**, 034311

Todd-Rutel,B.G., Piekarewicz,J. 2005, *Phys.Rev.Lett.*, **95**, 122501

Tolman,R.C. 1939, *Phys.Rev.*, **55**, 364

Tu,Z.H., Zhou, S.G., 2022, *Astrophys.J.*, **925**, 16

Typel,S., Wolter,H.H. 1999, *Nucl.Phys.A*, **656**, 331

Weissenborn,S., Chatterjee,D., Schaffner-Bielich,J. 2012, *Nucl.Phys.A*, **881**, 62

Zhao,X.F. 2019, *Int.J.Theor.Phys.*, **58**, 1060

Zhou,S.G. 2016, *Phys.Scr.*, **91**, 063008

Zhou, Y., Chen, L.W.: 2019, *Astrophys.J.*, **886**, 52